Phytotherapy Research

WILEY

RESEARCH ARTICLE OPEN ACCESS

Angelica dahurica Polysaccharides Ameliorate Colitis by Reducing the Restriction of Gut Microbiota-Derived Imidazole Propionate on PPAR-γ Signaling Activation

Jingyi Hu[1] | Feng Xu[2] | Lei Zhu[1] | Yuan Cui[2] | Ryan Au[3] | Yanan Li[2] | Yiheng Tong[2] | Hong Shen[1]

[1]Affiliated Hospital of Nanjing University of Chinese Medicine (Jiangsu Province Hospital of Chinese Medicine), Nanjing, China | [2]First Clinical Medical College, Nanjing University of Chinese Medicine, Nanjing, China | [3]International Education College, Nanjing University of Chinese Medicine, Nanjing, China

Correspondence: Hong Shen (shenhong999@njucm.edu.cn)

Received: 30 March 2024 | **Revised:** 19 August 2024 | **Accepted:** 21 August 2024

Funding: This work was financially supported by the National Natural Science Foundation of China [grant 82274483 to H.S., and 82205023 to J.H.], High-level Key Discipline Project of Traditional Chinese Medicine (Spleen and Stomach Diseases of Traditional Chinese Medicine) of the State Administration of Traditional Chinese Medicine (Guozhong Pharmaceutical Renjiao Letter (2023) No. 85) to H.S., Jiangsu Provincial Innovation Center for Traditional Chinese Medicine Digestive Medicine (Suwei Kejiao (2022) No. 15) to H.S., the Youth Talents project of Jiangsu Administration of Traditional Chinese Medicine [grant nos. QN202106] to J.H., Outstanding Young Doctor Training Program of Jiangsu Province Hospital of Chinese Medicine [2023QB0132] to J.H., and the Postgraduate Research & Practice Innovation Program of Jiangsu Province [grant nos. KYCX22_1938] to F.X.

Keywords: *Angelica dahurica* polysaccharides | gut microbiota | imidazole propionate | PPAR-γ signaling

ABSTRACT

Angelica dahurica radix (ADR), the root of the botanical family *Apiaceae* (genus *Angelica*, species *Angelica dahurica* (*Hoffm.*)), has been used to treat colitis in clinical practice. The immunomodulatory effects of ADR are attributed to its polysaccharides (RP). However, its mechanism of action has not been elucidated. In this study, RP's structure was determined through nuclear magnetic resonance analysis. Dextran sulfate sodium-induced colitis in mice was utilized to assess the therapeutic efficacy of RP, while experiments involving fecal microbiota transplantation (FMT) and antibiotic treatment were performed to investigate the contribution of gut microbiota to RP's protective function. Non-targeted metabolomics was utilized to identify potential targets for elucidating the underlying mechanisms. RP is likely composed of (→4)-α-D-Glcp-(1→ and →4)-α-D-Galp-(1→). It effectively alleviated DSS-induced colitis by restoring the balance of the gut microbial community, a finding validated through FMT and antibiotic intervention experiments. Imidazole propionate (ImP) emerged as a potential target for RP's efficacy in treating colitis, which inhibits the activation of peroxisome proliferator-activated receptor gamma (PPAR-γ). Our findings suggest that RP may confer protection against colitis by activating the PPAR-γ signaling pathway through alleviating the constraint imposed by ImP.

1 | Introduction

Ulcerative colitis (UC) is a primary sort of inflammatory bowel disease (IBD) (Magro et al. 2017). The lesion is situated within the mucosal and submucosal layers of the rectum and colon, resulting in hematochezia and abdominal discomfort. The global incidence of UC is on the rise, leading to a corresponding escalation in healthcare expenditures (Ng et al. 2017). Environmental and genetic factors are known to play a central role in its etiology. Abundant research has demonstrated that alterations in the intestinal flora of UC patients modulate host immunity through metabolic signaling (Aonghus and Harry 2020). The alteration of

Jingyi Hu, Feng Xu, and Lei Zhu contributed equally to this work.

microbial metabolites, such as bile acids (BAs) (Guo et al. 2016), amino acids (AAs) (Shin et al. 2020), and short-chain fatty acids (SCFAs) (Sun et al. 2016), is the trigger for the development of UC. Re-establishing the microbial community through fecal microbiota transplantation (FMT) (Cammarota and Ianiro 2019; D'haens and Jobin 2019) or medication to restore the homeostasis of host-intestinal interaction is a promising therapy for UC. However, the mechanism underlying microbial metabolites in UC is still largely unknown.

The root of *Angelica dahurica Radix* (ADR, Baizhi in Chinese) has been recorded to have a potential therapeutic effect on intestinal disorders, especially those involving mucosal injury (Hu et al. 2021; Hwang et al. 2017). In the past decades, ADR has attracted far-reaching attention in colitis treatment. Many studies have isolated and identified the active constituents in ADR, and plenty of compounds, including imperatorin (Liu et al. 2018), kaempferol (Qu et al. 2021), and β-sitosterol (Zhang et al. 2023), have shown extraordinary effects on colitis treatment via immunity signals. However, new drug discoveries from ADR often focus on small molecule compounds, and macromolecular compounds, such as polysaccharides and proteins, are usually ignored. According to various reports, water-soluble polysaccharides are the main compounds derived from the water-extraction of ADR (Wang et al. 2017), and have been shown to have biological activity, including immune regulation, antitumor, and antiviral effects (Wang et al. 2017; Xu et al. 2011). We previously found that water-extracted ADR could attenuate colitis by promoting the recovery of the mucosal barrier depending on intestinal flora (Hu et al. 2021). Considering the solubility of compounds, we isolated the polysaccharides from water-extracted ADR, named RP, and hypothesized that RP would ameliorate dextran sodium sulfate (DSS)-induced colitis by rebalancing the metabolites secreted from the gut microbiota to regulate intestinal immunity. Here, we report that RP significantly mitigated colitis severity, gut microbiota dysbiosis, and metabolic imbalance. We revealed that RP alleviated the restriction of gut microbiota-derived imidazole propionate (ImP) on PPAR-γ signaling activation.

2 | Materials and Methods

2.1 | Reagents

DSS (MW: 36–50 k, Cat# 160110) was bought from MP Biomedicals (Burlingame, USA). RP was purchased from Weikeqi Biological Technology (Chengdu, China). 3-(1H-Imidazol-4-yl)-propionic acid (IMP, Cat# I165812) was obtained from Aladdin (Shanghai, China). ChamQ SYBR Master Mix for qPCR (Cat# Q311-02/03), RT SuperMix for qPCR (Cat# R323-01), and RNA isolation kit (Cat# R711) were purchased from Vazyme Biotech (Nanjing, China). FITC-dextran (4 kDa; average MW 3000–5000, Cat# 46944, CAS: 60842–46-8) was bought from Sigma-Aldrich (St. Louis, MO, USA). β-actin (Cat# 66009–1-Ig), HRP-conjugated Goat-Anti-Mouse IgG (Cat# SA00001–1), HRP-conjugated Goat Anti-Rabbit IgG (Cat# SA00001–2), and Apolipoprotein AI Polyclonal antibody (ApoA1, Cat# 14427-1-AP) were bought from Proteintech Group (Rosemont, USA). Anti-ZO-1 (Cat# GB111981) and Anti-MUC2 (Cat# GB14110) were obtained from Servicebio Biotech (Wuhan, China). Anti-PPARγ (Cat# 2435) was obtained from Cell Signaling Technology (Danvers, USA). Anti-Claudin4 (Cat# ab15104) was bought from Abcam (Cambridge, UK). Super-sensitive ECL chemiluminescent substrate was purchased from Labgic Technology (Beijing, China). Myeloperoxidase (MPO, Cat# EK2133), tumor necrosis factor-alpha (TNF-α) (Cat# EK282), interleukin-1β (IL-1β) (Cat# EK201B), and IL-6 (Cat# EK210) ELISA kits were purchased from Multi Sciences (Shanghai, China). Fetal Bovine Serum (Cat# C04001) and RPMI-1640 (Cat# C30100) were obtained from Biological Industries. The CCK-8 Cell Counting Kit (Cat# A311-01) was obtained from Vazyme Biotech (Nanjing, China).

2.2 | Chemical Analysis

The total carbohydrate content was analyzed by the phenol–sulfuric acid method. The glucuronic acid content was benchmarked by the meta-hydroxydiphenyl method (Blumenkrantz and Asboe-Hansen 1973).

2.3 | Determination of Molecular Weight (Mw)

The Mw of RP was ascertained by high-performance gel permeation chromatography (HPGPC) on a Shimadzu LC-10A series apparatus equipped with a BRT105-103-101 column (8 × 300 mm) and a refractive index detector. The mobile phase used was 0.2 M sodium chloride flowing at a rate of 0.8 mL/min at 40°C. Dextran standards (Mw 5.9, 9.6, 21.1, 47.1, 107, 200, 344, and 708 kDa) were utilized to create the calibration curve for calculating the Mw.

2.4 | Monosaccharide Composition Analysis

The monosaccharide composition of RP was analyzed according to a previous report (Zhu et al. 2021). About 10 mg of RP was hydrolyzed (121°C, 2 h) using 2 mL trifluoroacetic acid (TFA, 2.5 mol/L). The surplus TFA was r eliminated by purging with nitrogen gas and methanol three times. The dried samples were melted in ddH_2O to prepare the specimen for analysis of high-performance anion-exchange chromatography (HPAEC). The equipment was equipped with pulsed amperometric detection (PAD) and consisted of an ICS-5000 system with a Dionex CarboPac PA20 (150 × 3 mm, 6.5 μm).

2.5 | Methylation Analysis

The RP's glycosidic linkage pattern was detected as in a previous study (Wold et al. 2018). About 20 mg of RP was dissolved in dimethyl sulfoxide (DMSO) (20 mg/mL). The solution was methylated using DMSO/NaOH with methyl iodide (CH_3I). The permethylated products were hydrolyzed with TFA (2 mol/L) at 121°C for 1.5 h, followed by reduction with $NaBD_4$, and finally acetylated with acetic anhydride (100°C, 2.5 h). The acetates were dissolved in chloroform and examined with gas chromatography–mass spectrometry (Agilent 6890A-5975C) with a chromatographic column (Agilent BPX70, 30 m × 0.25 mm × 0.25 μm). High-purity helium (split ratio 10:1) served as the carrier gas with an injection volume of 1 μL. The

initial temperature for the mass spectrometry analysis was set at 140°C for 2 mins, followed by a stepwise increase to 230°C at a rate of 3°C/min. The injection temperature and the detector temperature were 260°C and 230°C, respectively. Helium was used as the carrier gas at 1 mL/min. Scan mode ranged from 50 to 350 (m/z).

2.6 | Nuclear Magnetic Resonance (NMR) Spectroscopy

About 20 mg of RP was dissolved in 500 μL D_2O. Signals for 1D-NMR (^{13}C-NMR and ^{1}H-NMR) and 2D-NMR including COSY, HMBC, NOESY, and HSQC were obtained using a Bruker AVANCE NEO 500 spectrometer. The spectrometer was equipped with a liquid probe QXI 1H/31P/13C/15 N 5 mm four resonance reverse detection probe (Z-gradient, ATM Acc) was used to acquire the mixing time of 0.6 s, and the signals were recorded at 25°C. Water peaks were used to calibrate the samples.

2.7 | Animals and Experimental Design

Male mice (C57BL6/J, 6 weeks old, SPF) were obtained from Vital River Laboratory Animal Technology (Zhejiang, China). During the experiment, the mice were kept in enclosures within a room that maintained a consistent temperature and humidity (25°C ± 1°C, 55% ± 5%) with a 12-h light/dark cycle. Animal experimental procedures were permitted by the Animal Ethics Committee in the Affiliated Hospital of Nanjing University of Traditional Chinese Medicine (Application Number: 2022DW–61–01) on December 12th, 2022.

2.7.1 | Established Chronic Colitis Model and RP Treatment

For RP treatment experiments, all mice were separated into 4 groups: Ctrl group, DSS group, DSS/RP-L (200 mg/kg), and DSS/RP-H (400 mg/kg), $n = 7$–10. The procedure for inducing colitis was identical to our previous research (Hu et al. 2021). Briefly, distilled water containing 2.0% DSS (w:v) was given to mice freely for 7 days, followed by another 14 days of distilled water. Following exposure to 3 cycles of DSS and water, mice were euthanized on day 64th. Weekly, the mice's body weight was documented.

2.7.2 | Fecal Microbiota Transplants (FMT) Experiment

For FMT or fecal microbiota transplant (FNT) experiments, all mice were separated into 6 groups: FMT-Ctrl group, FMT-DSS group, FMT-RP group, FNT-Ctrl group, FNT-DSS group, and FNT-RP group, $n = 6$–10. FMT treatment for colitis mice was performed according to a previous report (Wu et al. 2021). Briefly, about 0.5 g of fresh feces from mice treated with or without RP were collected and pooled in 10 mL sterile phosphate-buffered saline (PBS) under anaerobic conditions. The fecal material was suspended by thorough vortexing (5 min) with a final concentration of 50 mg feces/mL. Then the samples were centrifuged (100 g, 5 min), and the supernatant was collected and filtered through 70-μm filters for FMT treatment. Mice in the FMT-Ctrl group and FMT-DSS group received the FMT from mice of the Ctrl group. Mice in the FMT-RP group received the FMT from mice in the RP group. For FNT treatment, the supernatant was filtered through a 70-μm filter, followed by a 0.22-μm filter. Mice in the FNT-Ctrl group and FNT-DSS group received the sterile fecal filtrate from the mice of the Ctrl group. Mice of the FNT-RP group received the sterile fecal filtrate from mice of the RP group. Mice were orally administered FMT or sterile fecal filtrate every day for 3 days before DSS intervention. The body weight of the mice was logged at the same time every day.

2.7.3 | Pseudo Germ-Free (PGF) Mice and Colitis Establishment

Mice were allocated into three groups: PGF-Ctrl, PGF-DSS, and PGF-RP, $n = 6$-8 with 10 mice in each group. The experimental method was adapted from a previous study (Hu et al. 2021). Briefly, all mice were treated with a mixture of four antibiotics comprised of metronidazole (0.5 g/L), neomycin sulfate (0.5 g/L), vancomycin hydrochloride (0.25 g/L), and sodium ampicillin (0.5 g/L) in their drinking water during the experiment. From Day 8 to Day 14, the drinking water of mice in the PGF-DSS and PGF-RP groups was supplemented with a 4% DSS solution combined with an antibiotic cocktail. Concurrently, mice were administered either distilled water or RP (200 mg/kg) orally. The body weight of the mice was logged at the same time every day.

2.7.4 | Acute Colitis Model and ImP Treatment

To evaluate the impact of ImP on the progression of colitis, 560 μg ImP was dissolved in 1 mL ddH_2O containing 10 μL DMSO to prepare an enema solution. Mice were randomly divided into the Ctrl group, ImP group, DSS group, and DSS/ImP group, $n = 7$–10 per group. Every morning, the mice were anesthetized with 0.5%–1.5% isoflurane until they reached a surgical plane of anesthesia, which was confirmed by a negative pedal reflex test. Subsequently, mice in the ImP and DSS/ImP groups received rectal administration of ImP (2.8 mg/kg), while those in the Ctrl or DSS groups were administered an equivalent volume of 1% DMSO rectally. The body weight of the mice was logged at the same time every day.

2.8 | Disease Active Index

The disease activity index (DAI) score was computed as previously reported (Cheng et al. 2022). The average was calculated based on the combined scores of body weight reduction, feces firmness, and rectal hemorrhaging. The criteria of the DAI score are shown in Table S1.

2.9 | Assessment of Intestinal Permeability

The intestinal permeability was detected using FITC-dextran. Following an overnight fast, mice were orally administered

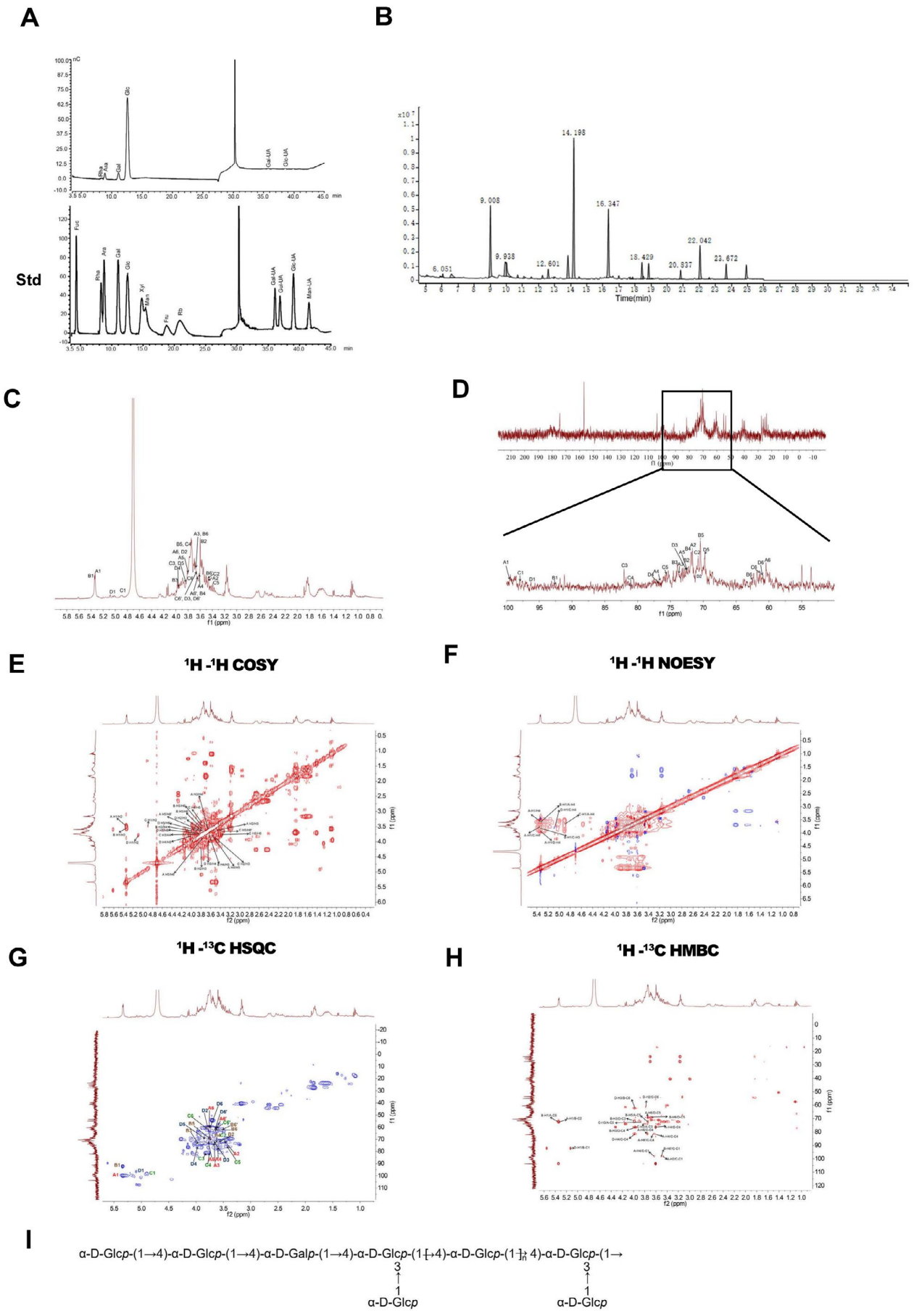

FIGURE 1 | Legend on next page.

FIGURE 1 | The chemical characterization of RP. (A) The monosaccharide composition of RP. (B) Gas chromatography–mass spectrometry (GC–MS) analysis of RP. (C, D) The ^{1}H NMR (C) and ^{13}C NMR (D). (E–H) HSQC (E), NOESY (F), HSQC (G), and HMBC (H). (J) Structure of RP.

TABLE 1 | Methylation analysis of RP.

Type of linkage	Methylated sugars	Retention time (min)	Molar ratio (%)
t-Ara(f)	1,4-di-O-acetyl-2,3,5-tri-O-methyl arabinitol	6.051	1.26
t-Glc(p)	1,5-di-O-acetyl-2,3,4,6-tetra-O-methyl glucitol	9.008	22.65
5-Ara(f)	1,4,5-tri-O-acetyl-2,3-di-O-methyl arabinitol	10.702	1.08
3-Glc(p)	1,3,5-tri-O-acetyl-2,4,6-tri-O-methyl glucitol	12.245	1.11
2-Glc(p)	1,2,5-tri-O-acetyl-3,4,6-tri-O-methyl glucitol	12.601	2.77
4-Gal(p)	1,4,5-tri-O-acetyl-2,3,6-tri-O-methyl galactitol	13.828	7.85
4-Glc(p)	1,4,5-tri-O-acetyl-2,3,6-tri-O-methyl glucitol	14.198	41.51
3,4-Glc(p)	1,3,4,5-tetra-O-acetyl-2,6-di-O-methyl glucitol	16.347	17.07
4,6-Glc(p)	1,4,5,6-tetra-O-acetyl-2,3-di-O-methyl glucitol	18.429	2.93
3,4,6-Glc(p)	1,3,4,5,6-penta-O-acetyl-2-O-methyl glucitol	20.837	1.77

FITC-dextran (20 mg/20 g). Serum samples were collected after 4 h for subsequent analysis. The level of FITC-dextran in serum was reckoned according to a standard curve.

2.10 | Histopathologic Analysis

Colonic samples were fixed in 4% paraformaldehyde and then encased in paraffin. After that, the colonic tissues were sectioned into thick specimens (4-μm), dyed with hematoxylin and eosin (H&E) or Alcian blue-periodic acid Schiff (AB-PAS), both of which were performed with the standard protocols using commercial kits (Servicebio Co. Ltd. Wuhan, China). Images were scanned. A pathologist scored the histology slides in a manner that was blinded.

2.11 | RNA Isolation and Quantitative Real-Time PCR (qRT-PCR)

Total RNA from the colonic tissue was isolated using a FreeZol Reagent (Vazyme, Cat# R711). The quantity and purity of RNA were estimated using Nanodrop. About 10 μL of RNA was used for reverse transcription by the PrimeScript RT Master Kit (Vazyme, Cat# Q611). The expression of the gene was measured using a LightCycler 96 Real-Time PCR detection system (Roche, Swiss). β-actin was used to normalize the analyses. All primers in this study were synthesized by Generay Biotech (Shanghai, China) (Table S2).

2.12 | Western Blot Analysis

The tissue or collected cells were dissolved in RIPA lysis solution containing 1 mM phenyl-methanesulfonyl fluoride (PMSF), and the concentration of proteins was measured by bicinchoninic acid assay. About 40 μg of protein were analyzed by SDS-PAGE using 8%–10% gradient polyacrylamide gels, and then wet-transferred onto polyvinylidene difluoride (PVDF) membranes. To further investigate the samples, immunoblotting was conducted using specific antibodies targeting claudin4, PPAR-γ, and APOA1 proteins, followed by secondary conjugated antibodies. Then, it was imaged with HRP substrate utilizing the ChemiDoc XRS+ system (Bio-Rad, USA).

2.13 | Immunofluorescence and Immunohistochemistry

2.13.1 | Immunofluorescence Analysis

Paraffin-embedded colonic sections were incubated with primary antibodies PPAR-γ (GB12164), ZO-1 (GB111402), and MUC2 (GB11344) at 4°C overnight. Nuclei were counterstained with DAPI stain (GDP1024, Servicebio, China). Immunostained images were observed using CaseViewer (Version 2.4; 3DHISTECH Ltd.).

2.13.2 | Immunohistochemistry

The paraffin sections were incubated with the primary antibody ZO-1 (GB111402) overnight at 4°C. Slides were washed three times in PBS before incubation with the secondary antibody (GB23303) for 20 min at 37°C.

2.14 | Measurement of Cytokines and MPO in Colonic Tissue

The level of cytokines and MPO in colonic tissue was assessed with Mouse ELISA kits following the provided guidelines. The final results were standardized based on the protein concentration in the colonic tissue.

TABLE 2 | ^{1}H and ^{13}C chemical shift values (δ in ppm) of RP.

Code	Glycosyl residues	Chemical shifts (ppm)					
		H1/C1	H2/C2	H3/C3	H4/C4	H5/C5	H6/C6
A	→4)-α-D-Glc*p*-(1→	5.33	3.48	3.65	3.61	3.8	3.78, 3.63
		99.55	71.65	73.77	76.27	72.46	60.44
B	α-D-Glc*p*-(1→	5.34	3.59	3.97	3.63	3.75	3.65, 3.5
		92.6	72.24	73.89	71.86	70.41	62.53
C	→3,4)-α-D-Glc*p*-(1→	4.9	3.49	3.82	3.75	3.4	3.81, 3.64
		98.09	70.78	82.07	81.07	75.69	61.2
D	→4)-α-D-Gal*p*-(1→	5.09	3.78	3.64	3.96	3.82	3.73, 3.64
		96.24	71.19	72.58	76.67	69.75	60.85

2.15 | Intestinal Flora Analysis

The content of the ileocecal valve of mice in the Ctrl, DSS, and DSS/RP-L groups was used for the analysis of gut microbiota. 16S rRNA gene sequencing was performed by Majorbio Biotechnology Co. Ltd. (Shanghai, China). The specific steps for 16S rRNA sequencing and data analysis are detailed in Supporting Information.

2.16 | Metabolomics Analysis

Colonic tissue of mice in the Ctrl, DSS, and DSS/RP-L groups was used for analysis. The metabolomic analysis was conducted by Metabo-Profile Co. Ltd. (Shanghai, China) following the protocol established in recent research (He et al. 2022). The specific steps for metabolomics analysis are detailed in Supporting Information.

2.17 | RNA Sequencing

Colonic tissue of mice in the Ctrl, ImP, DSS, and DSS/ImP groups was used for the RNA sequencing. The RNA sequencing was performed by LC-Bio Technologies Co. Ltd. (Hangzhou, China). The detailed steps for RNA sequencing are provided in Supporting Information.

2.18 | Cell Culture and Treatment

NCM460, the epithelial cell line of human colon, was maintained in fixed conditions (5% CO_2, 37°C). The culture medium is RPMI-1640 containing 10% fetal bovine serum (FBS) and 1% penicillin/streptomycin. Cells were seeded in 96-well plates at a density of 1×10^4 cells per well or in 12-well plates at a density of 1×10^5 cells per well and cultured until reaching 80% confluence. Subsequently, the cells were treated with varying concentrations of ImP for 12 h. The viability of the cells was assessed with the cell counting kit (CCK)-8 according to the manufacturer's instructions.

2.19 | Statistical Analysis

Statistical analysis was implemented using Prism 8.0 (GraphPad Software). The data are displayed as mean ± SEM. A one-way analysis of variance (ANOVA) or two-way ANOVA was conducted to assess the statistical variance among groups, and $p < 0.05$ indicates significance.

3 | Results

3.1 | Structural Characterization of RP

RP was found to have a carbohydrate content of 90%, making it a neutral polysaccharide devoid of uronic acid. To determine the structure of RP, we first confirmed that RP was a homogeneous polysaccharide using HPGPC (Figure S1A). The Mw of RP was 3.037 kDa, while the average molecular weight (Mn) of RP was 2.882 kDa. The composition of RP included Rha, Ara, Gal, Glc, Glc-UA, and Gal-UA in a molar ratio of 0.61:5.76:5.73:85.58:0.82:1.49 (Figure 1A). It showed that RP was principally composed of glucose as a glucan. The glycosidic linkages of RP were identified through methylation analysis (Figure 1B). As shown in Table 1, RP contained 10 main glycosidic linkages. The structure of RP was further determined by 1D-NMR, including ^{1}H and ^{13}C NMR (Figure 1C,D), and 2D-NMR, including HSQC, COSY, HMBC, and NOESY (Figure 1E–H). According to the relevant literature, the characteristic proton and carbon signals of the residues A, B, C, and D in RP were confirmed based on the chemical shifts (Table 2) (Liang et al. 2022; Lopes et al. 2017; Wang, Cao, et al. 2019). In the ^{1}H spectrum of RP, the distinct peaks at δ 5.33, 5.34, 4.9, and 5.09 were assigned to the H-1 of the →4)-α-D-Glcp-(1→, α-D-Glcp-(1→, →3,4)-α-D-Glcp-(1→, →4)-α-D-Galp-(1→ residues in RP, respectively. The ^{13}C NMR spectrum showed anomeric carbon signals at δ 99.55, 92.6, 98.09, and 96.24, which corresponded to the C-1 of residues A, B, C, and D, respectively. The remaining oxygenated carbon signals fell within the 60–80 ppm range, thereby confirming their positioning between the C-2 and C-6 of the four residues. In the HSQC spectrum of residue A (Figure 1G), a relatively intense cross-coupling resonance signal at δ 5.33/99.55 ppm was

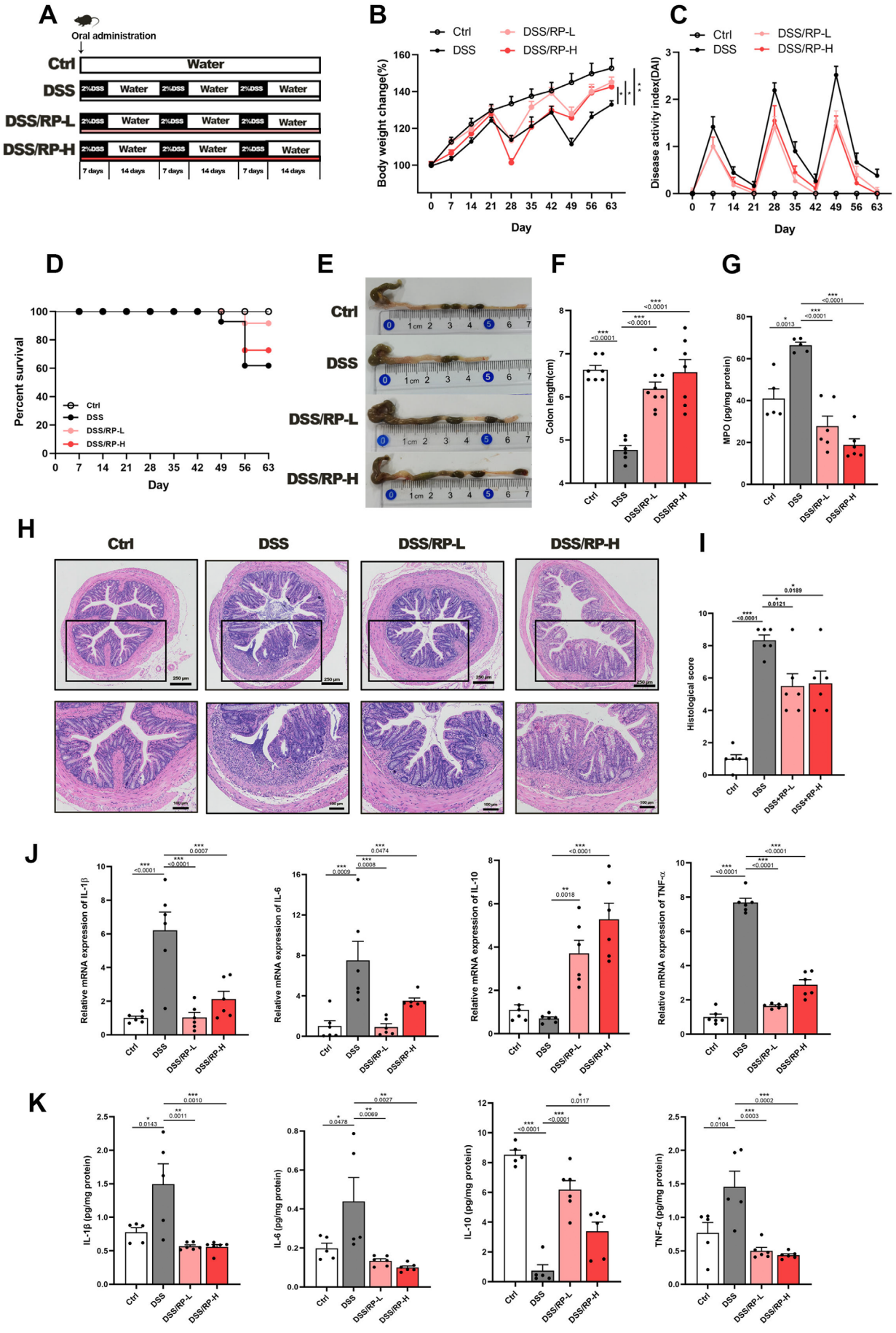

FIGURE 2 | Legend on next page.

FIGURE 2 | RP attenuates chronic colitis in mice. (A) The design of experiment. (B) Change of body weight during the experiment. (C) Change of disease active index (DAI) scores during the experiment. (D) The survival curve of the mice. (E, F) Representative images of the colons (E), and the average colon length for each group on day 64 (F). (G) The level of MPO in the colonic smaples in each group. (H, I) Representative H&E-stained of colon section (scale bar, 250 μm or 100 μm) (H) and histological score (I). (J) Relative mRNA expression of *Il1β*, *Il6*, *Il10*, and *Tnfα* in the colonic samples of mice. (K) Protein level of IL-1β, IL-6, IL-10, and TNF-α in the colonic tissue. Data are denoted as the mean ± SEM. $^{*}p < 0.05$, $^{**}p < 0.01$, $^{***}p < 0.001$.

assigned to A1 in the anomeric region of residue A. In addition, characteristic carbon chemical shift signals were observed at 3.48/71.65, 3.65/73.77, 3.61/76.27, 3.8/72.46, 3.78/60.44, and 3.63/60.44, corresponding to A2, A3, A4, A5, A6, and A6', respectively. Similarly, the results (Figure 1G, Table 2) were also observed for residues B, C, and D.

Based on the chemical shifts of various sugar residues in the ^{13}C and ^{1}H NMR (Figure 1C,D) spectra, combined with the HMBC spectra (Figure 1H), the structure and connection mode of the polysaccharide were analyzed. We identified a cross peak between sugar residue A-H4 and residue C-C1 δ 3.61/98.09 ppm. Furthermore, based on the NOESY spectrum (Figure 1F), it was inferred that there is a cross peak between sugar residue A-H1 and residue A-H4, indicating the connection order of each residue in the polysaccharide δ 5.34/3.61 ppm, a cross peak with residue C-H4 (δ 5.34/3.75 ppm), and a cross peak with residue D-H4 (δ 5.34/3.96 ppm). There is a cross peak between sugar residue B-H1 and residue A-H4 (δ 5.34/3.61 ppm), and a cross peak with residue C-H3 (δ 5.34/3.82 ppm). There is a cross peak between sugar residue C-H1 and residue A-H4 (δ 4.9/3.61 ppm). There is a cross peak between sugar residue D-H1 and residue C-H4 (δ 5.09/3.75 ppm). Thus, the possible structure of this polysaccharide chain is presented in Figure 1I.

3.2 | RP Attenuates Chronic Colitis

To assess the potential therapeutic efficacy of RP, we induced chronic colitis in mice using a chemical method (Figure 2A). Severe inflammation is a common outcome after subjecting them to repeated cycles of 2% DSS treatment. In the DSS/RP groups, the mice exhibited alleviation of colitis symptoms, including a reduction in the loss of body weight and an improvement in DAI score (Figure 2B,C). The mortality rate of the DSS/RP groups was lower than that of the DSS alone group (Figure 2D). RP treatment prevented colonic shortening in colitis mice and improved histological alteration (Figure 2E–I). Significantly, RP treatments suppressed the inflammatory response in the colon by decreasing the levels of pro-inflammatory cytokines and increasing the levels of anti-inflammatory cytokines (Figure 2J,K). Moreover, RP has been shown to exhibit hepatoprotective effects in colitis mice (Figure S2). Taken together, these results suggest that RP has a therapeutic effect on colitis.

3.3 | RP Restores Intestinal Barrier Function

Next, we evaluated the protective effect on the intestinal barrier, both in the mucosal barrier and physical barrier. The intervention of RP increased the number of goblet cells and the mucosal layer's thickness, possibly due to the increased expression of MUC2 (Figure 3A,B). Tight junctions (TJs), such as Occludin, ZO-1, and Claudin4, are critical components of the physical barrier. There was no discrepancy in expression between healthy and colitis mice, and a high dose of RP treatment prominently upregulated the expression of ZO-1 and Claudin 4 both at mRNA and protein levels (Figure 3C–G). These results indicate that RP could enhance the intestinal barrier.

3.4 | RP Rebalances the Construction of Intestinal Flora

Colitis is traditionally associated with dysbiosis. To investigate the regulatory impact of RP on the intestinal microbiota, we employed 16S rRNA gene amplicon sequencing. The structure of the intestinal flora was probed by unweighted UniFrac-based principal coordinates analysis (PCoA) and partial least squares (PLS)-discriminant analysis (PLS-DA) (Figure 4A,B). We noted that RP treatment could remarkably shift the structure of the intestinal flora, which was distinct from either the Ctrl or DSS groups. Moreover, Chao and Shannon indices, the α-diversity analysis, revealed that RP treatment prevented the decrease in gut microbiota richness (Figure 4C,D). We then further analyzed the composition of the intestinal flora at the phylum level (Figure 4E), and the results showed that RP could dramatically reduce the higher relative abundance of Proteobacteria (Figure 4F). Further analysis at the genus level showed that *Ileibacterium*, *nonran_o_clostridia_UCG-014*, and *Rikenella* play key roles in the RP-treated group, while *Blautia*, *Akkermansia*, *norank_f_Eubacterium_coprostanoligenes_group*, *Faecalibaculum*, and *Mucispirillum* were significantly increased in colitis mice (Figure 4G,H). These results show that RP treatment could rebalance the dysbiosis in colitis mice.

3.5 | The Protective Effects of RP on Colitis Rely on the Intestinal Flora

Next, the underlying role of the intestinal flora on the therapeutic effect of RP was analyzed using FMT or FNT (Figure 5A). In mice from the FMT-RP group, an increase in body weight and colon length was observed, along with a decrease in DAI scores compared to those from the FMT-DSS group (Figure 5B–D). However, there were no discernible differences in the symptoms of colitis between the FNT-DSS group and the FNT-RP group. In contrast, the FMT-RP group exhibited enhanced intestinal barrier function compared to both the FMT-DSS and FNT-RP groups (Figure 5E,F). Moreover, PGF mice were used to confirm the role of the gut microbiota in RP treatment (Figure 5G–L). Collectively, these findings indicate that the therapeutic efficacy of RP in treating colitis is contingent upon the composition of the gut microbiota.

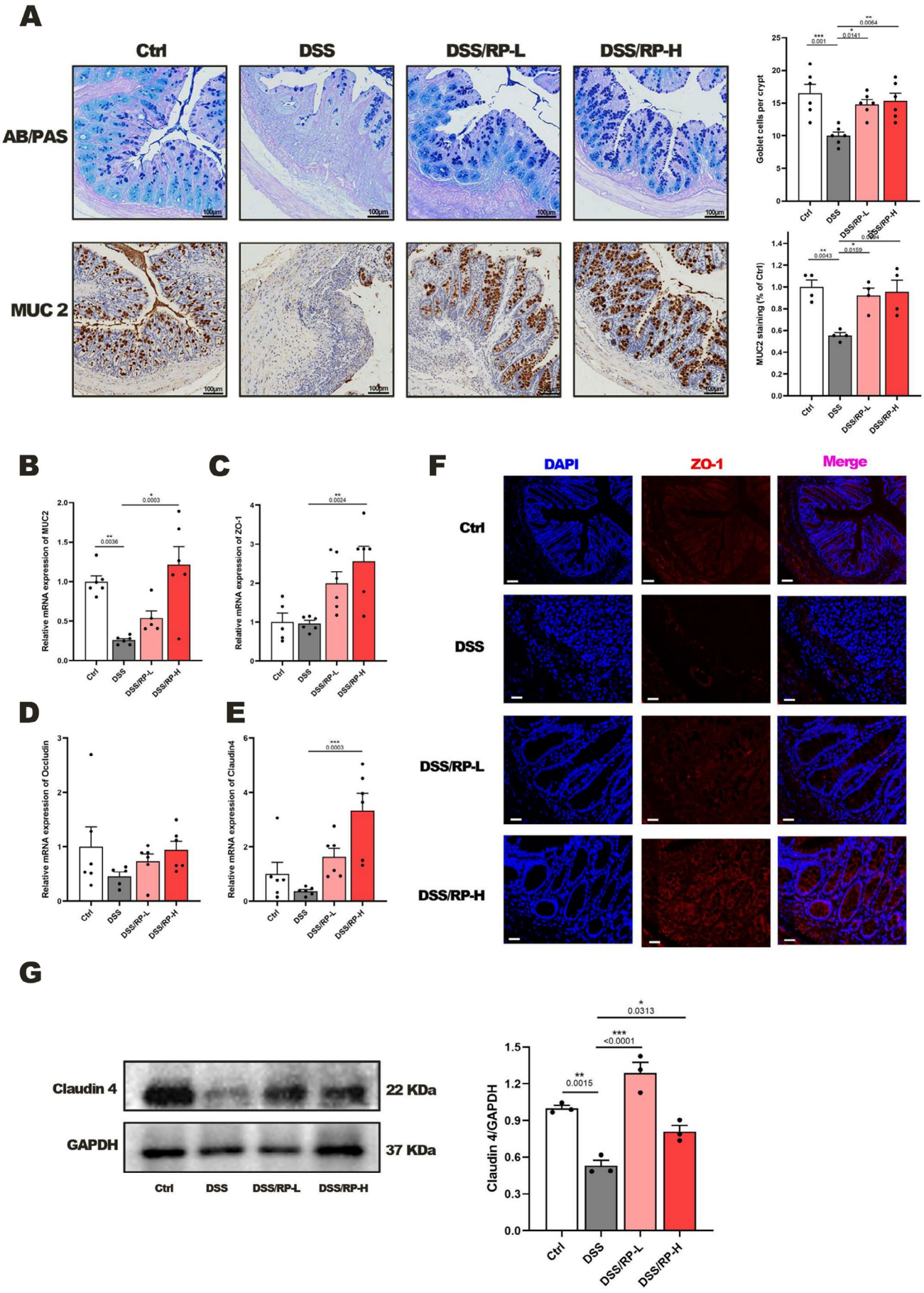

FIGURE 3 | Legend on next page.

FIGURE 3 | RP restores the intestinal barrier function. (A) Representative AB/PAS-stained colonic tissue section (scale bar, 100 μm), the number of goblet cells in the crypt, and immunohistochemical detection of proteins related to MUC2 in colonic sections (scale bar, 100 μm). (B) Relative mRNA expression of *Muc2* in the colon tissue of mice. (C–E) Relative mRNA expression of *Zo1* (C), *Occludin* (D), and *Claudin4* (E) in the colon tissue of mice. (F) Representative images of ZO-1 in colonic sections (scale bar, 100 μm). (G) Immunoblots of Claudin4 in the colonic tissue of mice. Data are denoted as the mean ± SEM. $^{*}p < 0.05$, $^{**}p < 0.01$, $^{***}p < 0.001$.

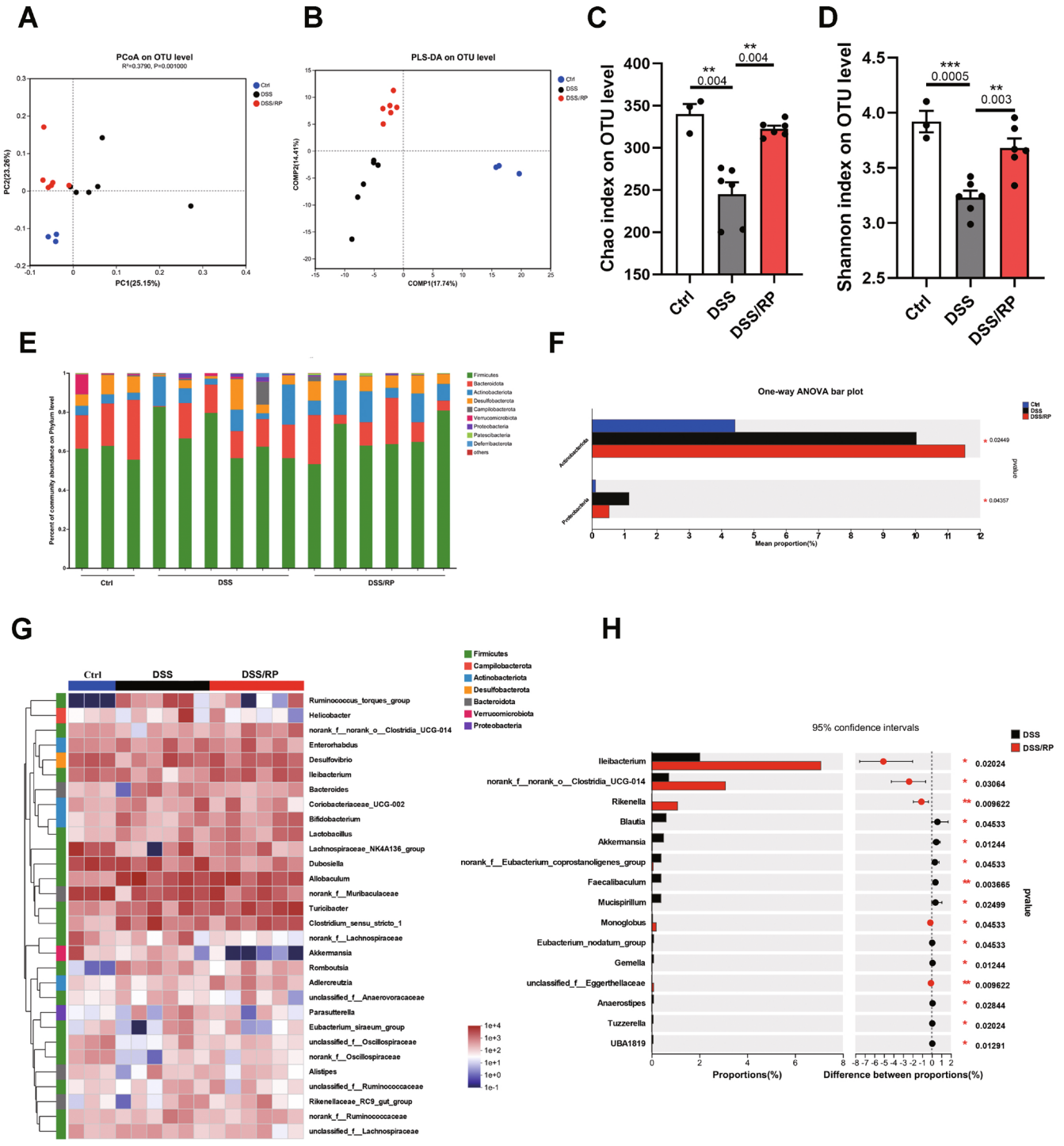

FIGURE 4 | RP rebalances the construction of gut microbiota. (A, B) Principal co-ordinates analysis (PCoA) plotting and partial least squares (PLS)-discriminant analysis (PLS-DA) plotting of the intestinal flora at the operational taxonomic unit (OTU) level. (C, D) Alpha diversity analysis of the intestinal flora richness (Chao index) and diversity (Shannon index) from different groups. (E) Bacterial taxonomic profiling at the phylum level. (F) Sequence tag-based analysis of microbial populations (STAMP) analysis of the differences among Ctrl, DSS, and RP-treated groups at the phylum level. (G) Bacterial taxonomic profiling of the intestinal flora at the genus level. (H) STAMP analysis of the differences between DSS and RP-treated groups at the genus level. Data are denoted as the mean ± SEM. $^{*}p < 0.05$, $^{**}p < 0.01$, $^{***}p < 0.001$.

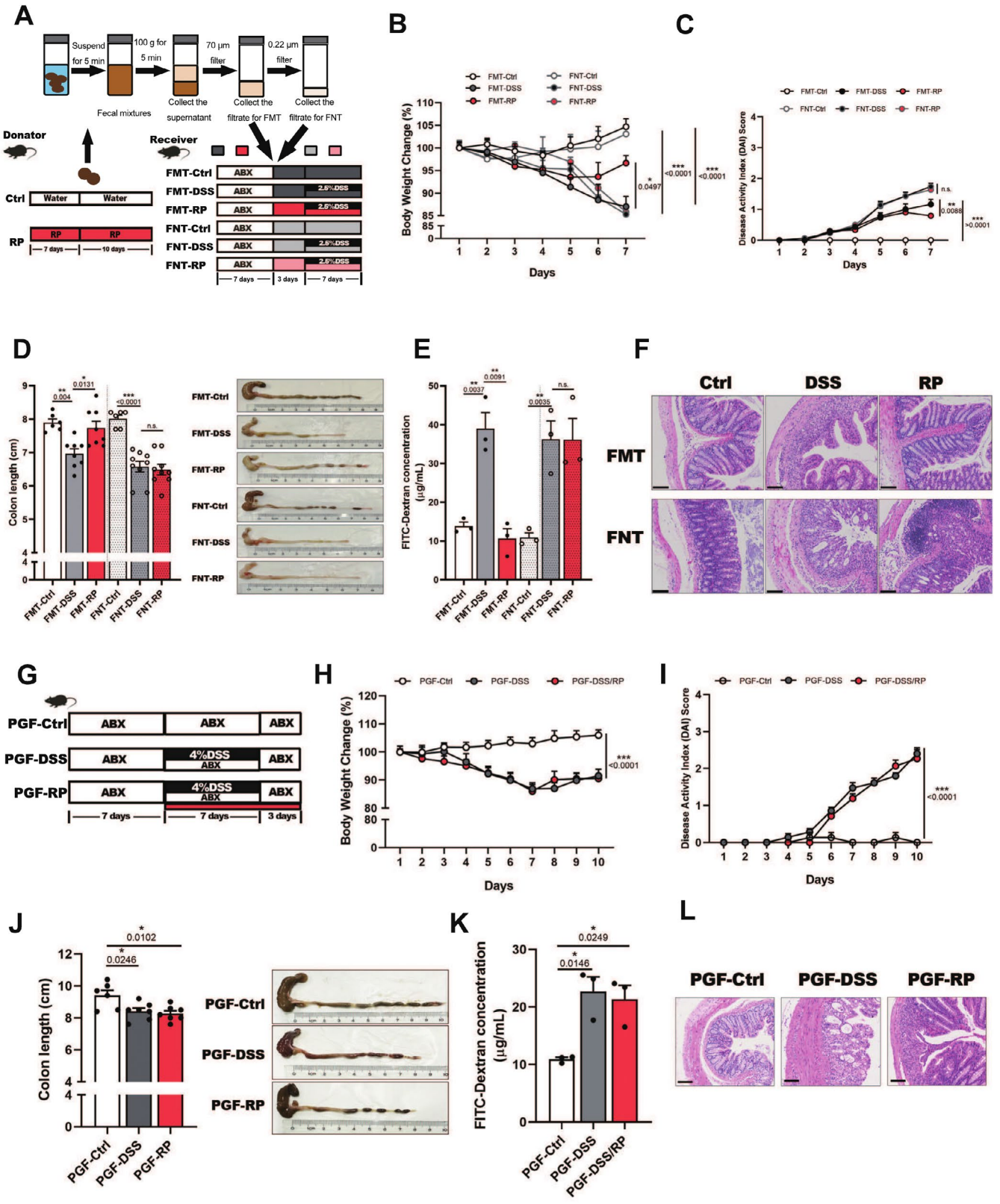

FIGURE 5 | The gut microbiota plays a core role in the effect of RP on colitis. (A) Experimental design of the fecal microbiota transplant (FMT) and the fecal no microbiota transplant (FNT) models. (B) Body weight changes during the experiment. (C) Disease active index (DAI) scores. (D) Representative images of colons, and the average colon length for each group. (E) Intestinal leakage was measured by serum FITC-dextran levels. (F) Representative H&E staining of colon tissue sections from each group. (G) Experimental design of DSS-induced colitis in pseudo-germ-free (PGF) mice. (H) Body weight changes during the experiment. (I) DAI scores. (J) Representative images of colons, and the average colon length for each group. (K) Intestinal leakage was measured by serum FITC-dextran levels. (M) Representative H&E staining of colon tissue sections from each group. Data are denoted as the mean ± SEM. $*p < 0.05$, $**p < 0.01$, $***p < 0.001$.

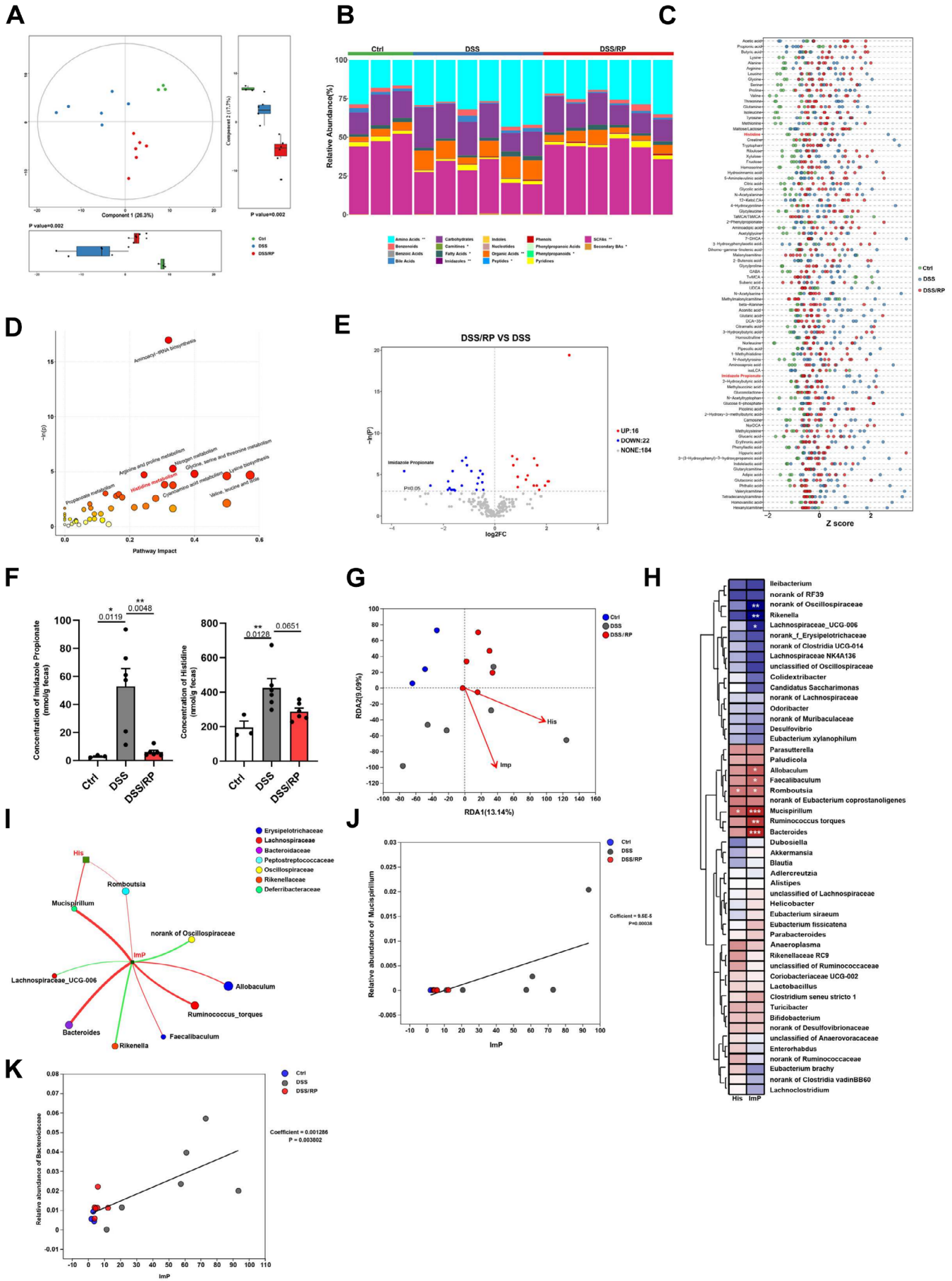

FIGURE 6 | Legend on next page.

FIGURE 6 | RP alters histidine metabolism and downregulates imidazole propionate. (A) The fecal metabolomic profiles were clustered using partial least squares (PLS)-discriminant analysis (PLS-DA). (B) Relative abundances of metabolites. (C) Relative abundances of potential biomarkers are shown in the *Z* score plot. (D) Metabolite pathway enrichment analysis of the metabolic biomarkers. (E) Volcano plot for differential metabolites between colitis mice and normal mice. (F) The concentration of fecal histidine (His) and imidazole propionic (ImP). (G) Procrustes analysis was used to superimpose distance-based redundancy analysis (dbRDA) ordinations of the indicated pairs of datasets. Ctrl, DSS, and DSS/RP samples are denoted by color. (H) Correlation analysis of the association of the RP-altered microbes and metabolites. (I) The dynamic association networks between gut microbes at the gene level and His and ImP. (J, K) Correlations were calculated in microbiome multivariable association with linear models (MaAslin). *Mucispirillum* (J) and *Bacteroidaceae* (K). Data are denoted as the mean ± SEM. $^{*}p < 0.05$, $^{**}p < 0.01$, $^{***}p < 0.001$.

3.6 | RP Alters Histidine Metabolism and Downregulates the Concentration of ImP

Microbial metabolites that play a vital role in host-microbiota interactions were changed following alteration of the intestinal flora. To assess the conversion of metabolites in response to RP treatment, metabolomic profiles were generated on colonic contents by UPLC-MS/MS. PLS-DA (Figure 6A) and principal component analysis (PCA) (Figure S3A) showed that the data points on the plots are widely dispersed. Metabolite classification indicated that the amino acids, carnitines, organic acids, and imidazoles were changed, and the relative quantities of fecal metabolites in all groups were visualized using a *Z*-score plot. The top 86 metabolites are listed in Figures 6B,C and S3B). Notably, histidine metabolism was the pathway that was significantly influenced by RP in the colonic contents (Figure 6D). The concentration of His and ImP (the gut metabolite of His) was significantly higher in the feces of colitis mice as compared with the Ctrl group, and RP treatment remarkably downregulated the concentration of ImP (Figure 6F).

An integrative analysis was performed to ascertain the potential correlation between modified gut microbiota and metabolites in RP-treated colitis mice. To test whether the therapeutic effect of *RP* on colitis mice is amalgamated with His, ImP, and the intestinal flora, distance-based redundancy analysis (Db-RDA) and Spearman correlation heatmap analyses were performed. As shown in Figure 6G, *RP* treatment was negatively correlated with His and ImP according to Db-RDA. Spearman correlation heatmap analysis revealed that ImP was highly positively correlated with *Allobaculum*, *Romboutsia*, *Mucispirillum*, *Ruminococcus torques*, and *Bacteroides* (Figure 6H,I). Consistently, maAslin analysis results showed that *Mucispirillum* and *Bacteroides* were positively correlated with ImP (Figure 6J,K). Taken together, these results show that RP treatment in colitis mice correlated with restoration of the intestinal flora and metabolism, especially the downregulation of ImP levels.

3.7 | ImP Directly Damages the Intestinal Barrier Function

The alteration of ImP in the feces is correlated to several diseases, such as diabetes mellitus (Koh et al. 2018). High levels of ImP may assist in the progression of colitis. Therefore, we evaluated whether ImP could damage the intestinal barrier integrity or promote inflammation. ImP administration alone or with DSS treatment was performed as Figure 7A. ImP alone did not directly influence the body weight of mice, DAI scores, or colon lengths (Figure 7B–F), and it did not cause an obvious infiltration of inflammatory cells. Moreover, there are no differences in pro-inflammatory cytokines in the Ctrl and ImP groups, indicating that ImP does not strictly induce colonic inflammation (Figure 7G,H). However, hyperpermeability of the intestinal barrier of mice in the DSS, ImP, and DSS/ImP groups was shown by FITC-dextran (Figure 7I). The mRNA and protein expression of *Zo1* and *Muc2* was significantly downregulated in these three groups (Figure 7J,K). These data demonstrate that ImP facilitates the permeability of the intestine, which may aggravate colitis.

3.8 | ImP Inhibits the PPAR-γ Signaling Pathway

To further delineate the mechanism underlying the increase in intestinal permeability in ImP-treated mice, we implemented genome-wide transcriptional profiling of the whole colonic tissues for RNA sequencing. We found noticeable differences between the ImP-treated and healthy mice (Figure 8A). There were 1184 genes were identified, with 574 genes increased and 610 genes decreased between Imp-treated mice and healthy mice (Figure 8B). Of note, PPAR signaling was one of the top two remarkably enriched functional pathways in ImP-treated mice according to Kyoto Encyclopedia of Genes and Genomes (KEGG) pathway analysis (Figure 8C,D). Moreover, there were 29 changed genes in the PPAR signaling pathway, such as lipid biosynthesis (*Fads2*), lipid transport (*Slc27a2*, *Slc27a4*), lipid binding (*Pparg*, *Ppara*, *Fabp6*, *Fabp2*, *Fabp1*), β-oxidation (*Cpt1a*, *Acsl3*, *Ehhadh*, *Cpt2*, *Acox1*, *Acaa1b*, *Acadm*), and cholesterol metabolism (*Hmgcs2*, *Apoa2*, *Apoa1*, *Apoa5*, *Acaa1a*, *Apoc3*, *Ppard*, *SCP2*, *Cyp4a31*, *Cyp4a12a*, *Cyp4a14*, *Cyp4a10*) (Figure 8E). Moreover, we used a search tool for recurring instances of neighboring genes (STRING) network to illustrate the interaction of remarkably changed genes in the PPAR signaling pathway (Figure 8F). Furthermore, the mRNA expression of *Pparg* and *Apoa1* was the most changed in ImP-treated mice compared with healthy mice (Figure 8G). The decreased protein expression of PPAR-γ and Apoa1 in colonic tissue with or without ImP treatment was confirmed using immunoblotting and immunofluorescence (Figure 8H,I), supporting the notion that ImP treatment induced inactivation of PPAR-γ during colitis. Also, we found that ImP could decrease the expression of *ZO1* and *Occludin* as well as inactivate the PPAR-γ pathway in vitro (Figure 8J–M). In contrast, giving RP could increase the expression of PPAR-γ (Figure S3). Overall, these results imply that ImP results in the variation of genes associated with lipid metabolism, and the inactivation of PPAR-γ signaling may result in damage to intestinal functions during colitis.

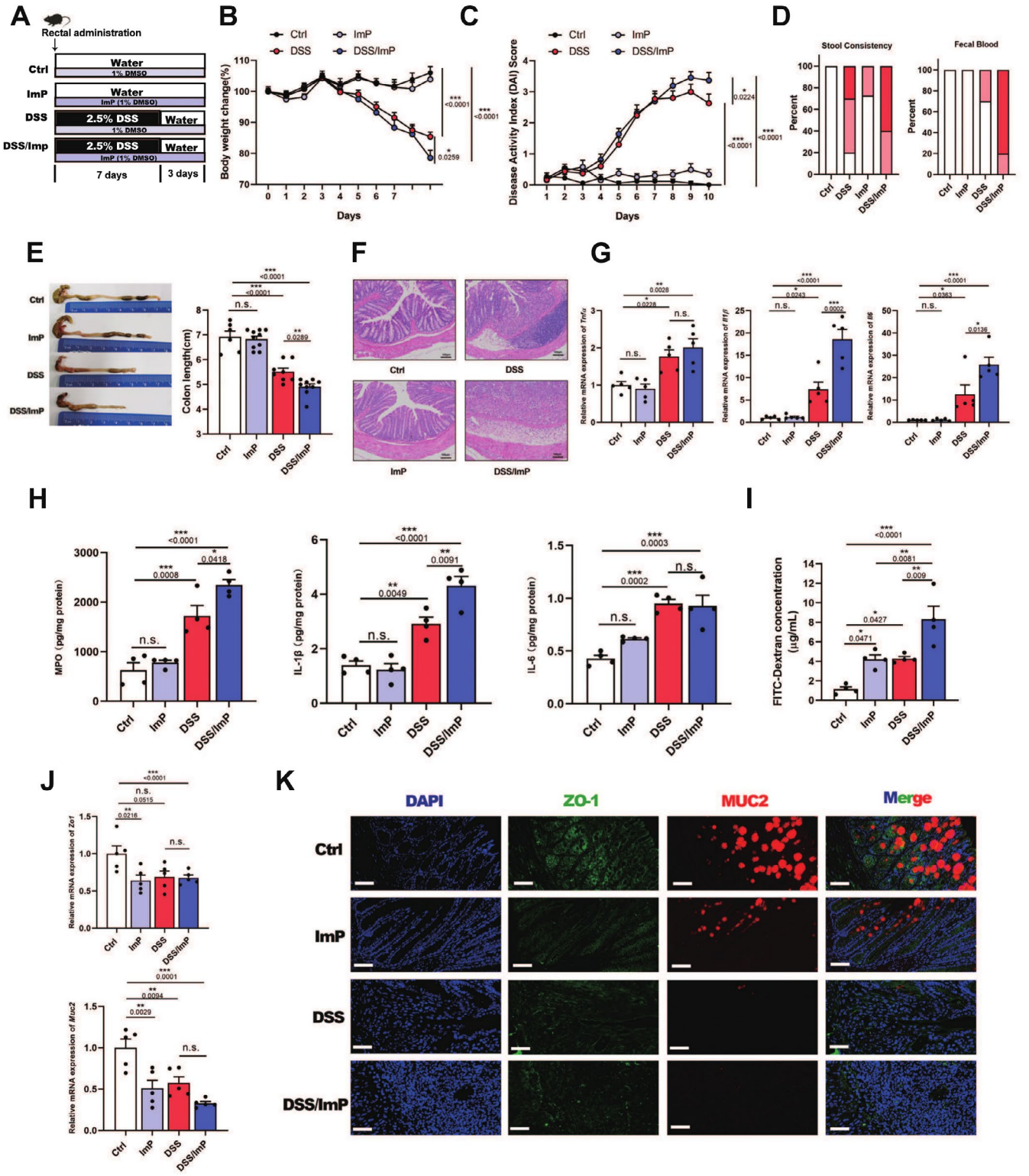

FIGURE 7 | ImP promotes DSS-induced acute colitis in mice. (A) The experimental design. (B) Body weight changes during the experiment. (C, D) Disease activity index (DAI) scores (C) and the other two factors of the DAI score, stool consistency and fecal blood (D). (E) Representative images of the colon, and the average colon length for each group. (F) Representative H&E-stained colon sections (scale bar, 100 μm). (G) Relative mRNA expression of *Il1β*, *Il6*, and *Tnfα* in the colonic tissue of mice. (H) The protein concentration of MPO, IL-1β, and IL-6 in the colonic tissue. (I) Intestinal leakage measured by serum FITC-dextran levels. (J) Relative mRNA expression of *Muc2*, *ZO1*, *and Occludin* in the colon tissue of mice. (K) Representative images of MUC2 and ZO-1 in the colonic section (scale bar, 50 μm). Data are denoted as the mean ± SEM. $^{*}p < 0.05$, $^{**}p < 0.01$, $^{***}p < 0.001$.

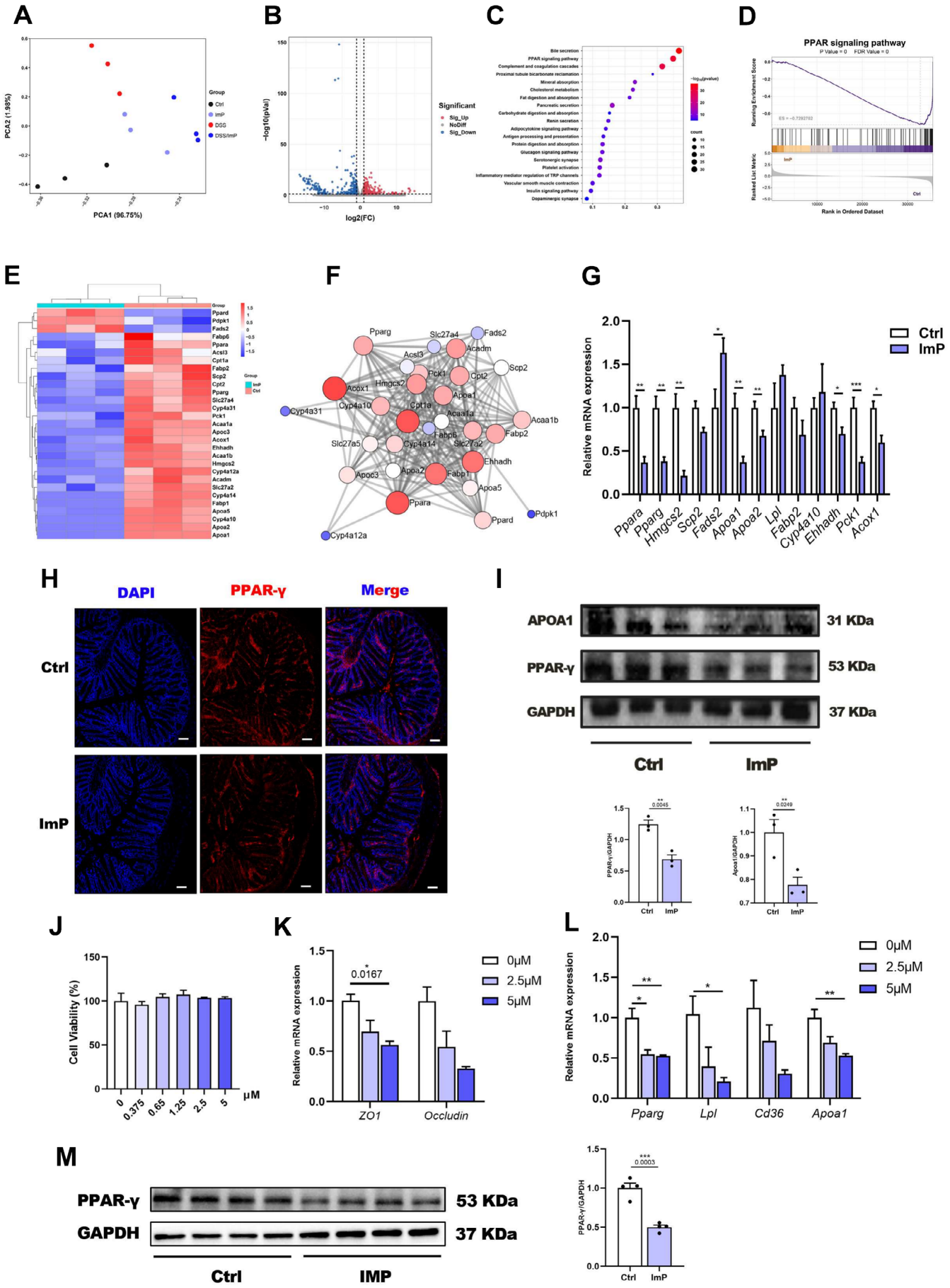

FIGURE 8 | Legend on next page.

FIGURE 8 | ImP alters gene expression in the murine colon and inhibits the PPAR-γ signaling pathway. (A) Principle component analysis (PCA) of transcriptional profiling. (B) Volcano plot for the differential gene between normal and ImP-treated mice. (C) Significantly changed pathways analysised by Kyoto Encyclopedia of Genes and Genomes (KEGG). (D) Gene set enrichment analysis (GSEA) of PPAR-γ signaling between the normal and ImP groups. (E) Different expressed genes in the PPAR signaling pathway between Ctrl group and ImP group. (F) Search tool for recurring instances of neighboring genes (STRING) network in the PPAR signaling pathway. (G) mRNA level of the differentially expressed genes in the PPAR signaling pathway. (H) Immunofluorescent analysis in colonic sections. PPAR-γ (red). Nuclei (blue); scale bar = 100 μm. (I) Immunoblot analysis of PPAR-γ and APOA1 in colonic tissue. (J) NCM460 cells were treated with ImP for 12 h, and cell viability analysis was detected by a CCK-8 assay. (J, K) NCM460 cells were incubated with ImP for 12 h, and the expression of tight junction genes and the PPARγ signaling pathway was examined by real-time PCR assay. (L) Immunoblot analysis of PPAR-γ in NCM460 cells. Data are denoted as the mean ± SEM. $^{*}p < 0.05$, $^{**}p < 0.01$, $^{***}p < 0.001$.

4 | Discussion

Gut dysbiosis represents the fundamental pathology underlying a multitude of diseases, including UC, and the interaction between gut microbiota and the host is increasingly garnering attention in clinical therapeutic strategies. Here, a glucan, Mw of 3.037 kDa and (→4)-α-D-Glcp-(1→ and →4)-α-D-Galp-(1→) structures, was purified from ADR. Through the investigation of the association between RP, a water-soluble polysaccharide of ADR, and the gut microbiota, we have identified ImP as a microbial metabolite that promotes the progression of colitis by inactivating the PPAR-γ pathway. Our findings provide a novel perspective on the therapeutic advantages of RP in clinical settings and elucidate a microbial-mediated metabolic pathway underlying intestinal epithelial injury.

For over two millennia across numerous Asian nations, ADR has been utilized for the treatment of intestinal disorders due to its proven efficacy in facilitating ulcer healing. Polysaccharides are one of the preponderant water-soluble ingredients of herbal medicine. The important role of herbal polysaccharides has been the subject of attention because of their bioactivity. Copious studies have previously shown that polysaccharides from ADR could suppress inflammation by regulating immune processes through TLR-dependent NF-κB transcription (Wang, Wang, et al. 2019). However, the potential involvement of microbial metabolism has not been covered. In combination with our previous study (Hu et al. 2021), a homogeneous polysaccharide from ADR was obtained. The RP had an Mw of 3.037 kDa with an (→4)-α-D-Glcp-(1→ and →4)-α-D-Galp-(1→) in its main chain. Plenty of literature reports showed that polysaccharides could regulate gut microbiota to relieve disease (Wang et al. 2022). The backbone of *Morchella esculenta* polysaccharide (Mw 959 kDa) is composed of →4)-α-D-Glcp-(1 → glucan and affects intestinal flora (Teng et al. 2023). Based on this evidence, we hypothesize that RP, the water-soluble polysaccharides from ADR, play a pivotal role in interacting with the gut microbiota, thereby modulating colonic immunity. In this study, we found that the therapeutic efficacy of RP against colitis was transferable by fecal transplantation, whereas it was blunted by sterile fecal filtrate transplantation or in gut microbiota-depleted mice. All these suggest that targeting the intestinal flora is a prospective frontier to elucidate the clinical effect of RP.

It is well known that metabolites are regulators of the crosstalk between the intestinal flora and the immune system of the host. In our study, metabolomic results showed new evidence that the dysregulated microbial production of ImP, an imidazole metabolite of His metabolism, aggravates colonic injury. Interestingly, a relationship between ImP and intestinal disorders in humans has been previously reported (Heiden et al. 1972). His and histamine 4 receptors are highly expressed in the mucosa of patients with UC (Smolinska et al. 2013; Wechsler et al. 2018), and ImP could be detected in the feces of patients with intestinal disorders, but was almost absent in the feces and urine from healthy subjects (Heiden et al. 1972). However, the specific bacteria involved in ImP production have not been fully elucidated. Some other studies found that high ImP and Bacteroides 2 enterotype levels have been linked to IBD (Molinaro et al. 2020; Vieira-Silva et al. 2019). Our results showed that two microbial genera, *Mucispirillum* and *Bacteroides*, were independently associated with higher fecal ImP levels. The current findings, in conjunction with prior research, indicate that the therapeutic efficacy of RP in a mouse model of colitis is contingent upon the modulation of intestinal flora, leading to the downregulation of high levels of *Mucispirillum* and *Bacteroides*, thereby restoring ImP homeostasis.

Although the correlation between ImP and colitis has been established, the precise role of ImP in the pathogenesis of UC remains elusive. Recent studies have suggested that microbial metabolites of His are immunomodulators in various diseases; for example, carotid artery atherosclerosis, type 2 diabetes, and colitis. An earlier report demonstrated that microbe-produced ImP was a pathogenic factor of type 2 diabetes and impaired glucose tolerance via activating the p38γ/p62/mammalian target of the rapamycin C1 (mTORC1) pathway (Koh et al. 2018). This study found that ImP treatment alone could remarkably damage tight junctions and mucosal function without causing inflammation. Moreover, RNA-sequencing data showed that the expression of the PPAR signaling pathway was significantly suppressed in the colonic tissue of mice treated with ImP when compared with normal mice. PPAR-γ is infinitely expressed in colonic tissue and plays a vital role in intestinal homeostasis (Byndloss et al. 2017). According to previous reports, the inactivation of PPAR-γ in the biopsy tissue of patients with colitis has been proposed as a vital event in colitis (Dubuquoy et al. 2003). Inadequate levels of natural ligands, such as butyrate and conjugated linoleic acid, have been proposed as the main reason for the inactivation of PPAR-γ signaling in colitis (Rousseaux et al. 2005). By supplementing exogenous PPAR-γ agonists or restoring endogenous PPAR-γ agonist levels, intestinal inflammation can be alleviated (Li et al. 2021; Stephanie et al. 2021). In this study, we highlight that ImP, a metabolic product of His produced in the gut microbiome, may damage intestinal barrier function by inactivating PPAR-γ signaling, suggesting that

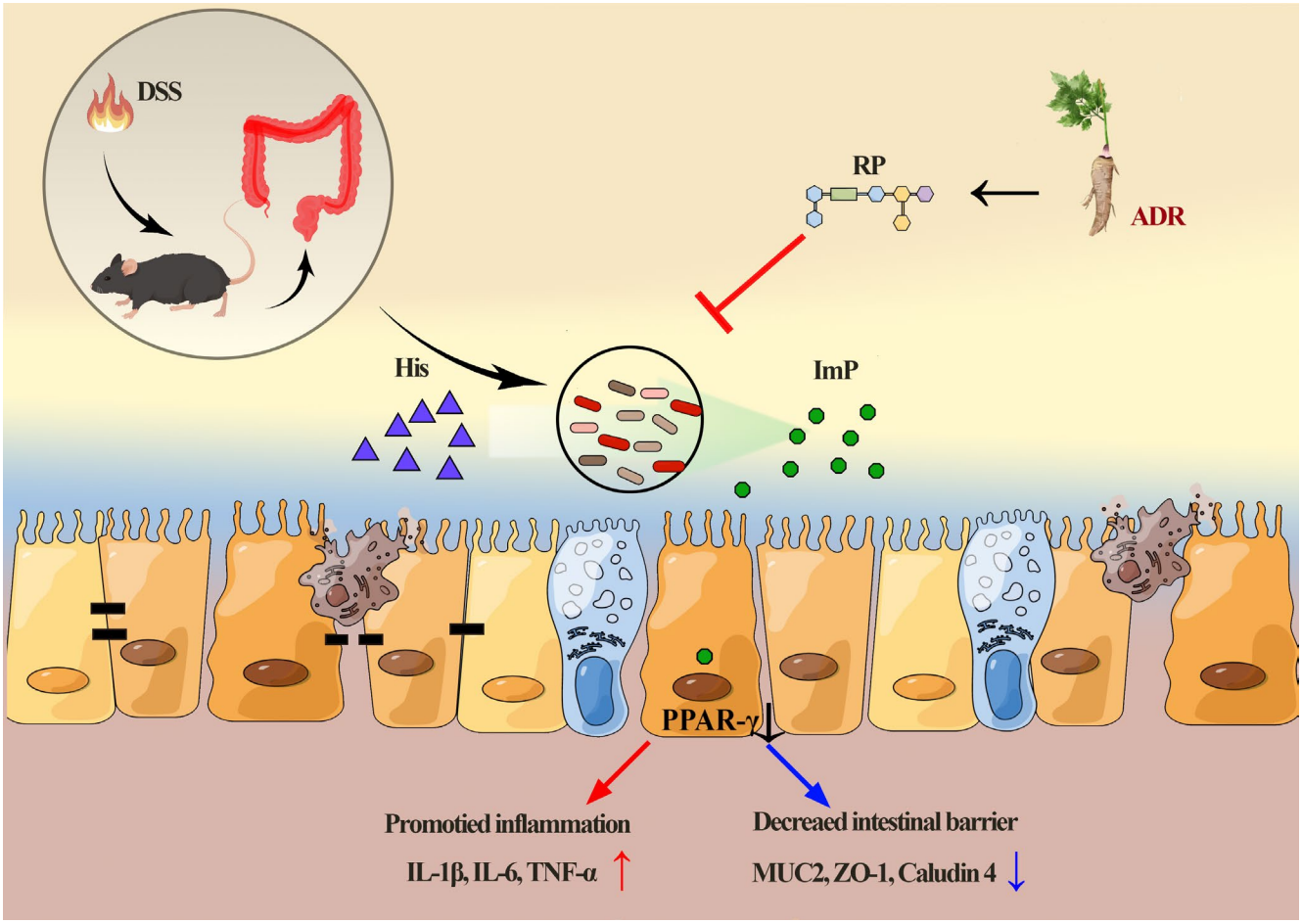

FIGURE 9 | Graphic abstract for the proposed microbiota-immune-regulating and colitis protecting effect of RP.

regulation of ImP metabolism may be a novel target for the treatment of colitis.

5 | Conclusions

In summary, the present study reports that RP, (→4)-α-D-Glcp-(1→ and →4)-α-D-Galp-(1→), exerts immunoregulation in colitis via gut microbiota-metabolism. Specifically, these regulatory effects were achieved through a gut microbiota-ImP-PPAR-γ signaling pathway. These findings suggest that the restoration of gut microbiota homeostasis and reduction in ImP levels may offer a promising therapeutic strategy for colitis (Figure 9). RP emerges as a potential candidate for the development of novel treatments for colitis.

Author Contributions

Jingyi Hu: investigation, supervision, writing – original draft. **Feng Xu:** data curation, methodology. **Lei Zhu:** formal analysis. **Yuan Cui:** methodology. **Ryan Au:** writing – original draft. **Yanan Li:** data curation. **Yiheng Tong:** software. **Hong Shen:** project administration, writing – review and editing.

Conflicts of Interest

The authors declare no conflicts of interest.

Data Availability Statement

The 16S rRNA datasets are available in the NCBI SRA database under the accession number PRJNA1065262. The metabolomic datasets have been deposited in the OMIX database with the identifier OMIX005755. The RNA sequencing data have been deposited in GEO with the subseries code GSE253817. Other datasets available from the current study are available from the corresponding author upon reasonable request.

References

Aonghus, L., and S. Harry. 2020. "Gut Microbiota-Derived Metabolites as Key Actors in Inflammatory Bowel Disease." *Nature Reviews Gastroenterology & Hepatology* 17, no. 4: 223–237. https://doi.org/10.1038/s41575-019-0258-z.

Blumenkrantz, N., and G. Asboe-Hansen. 1973. "New Method for Quantitative Determination of Uronic Acids." *Analytical Biochemistry* 54, no. 2: 484–489. https://doi.org/10.1016/0003-2697(73)90377-1.

Byndloss, M. X., E. E. Olsan, F. Riva-Chávez, et al. 2017. "Microbiota-Activated PPAR-γ Signaling Inhibits Dysbiotic Enterobacteriaceae Expansion." *Science* 357, no. 6351: 570–575. https://doi.org/10.1126/science.aam9949.

Cammarota, G., and G. Ianiro. 2019. "FMT for Ulcerative Colitis: Closer to the Turning Point." *Nature Reviews Gastroenterology & Hepatology* 16, no. 5: 266–268. https://doi.org/10.1038/s41575-019-0131-0.

Cheng, C., J. Y. Hu, Y. N. Li, et al. 2022. "Qing-Chang-Hua-Shi Granule Ameliorates DSS-Induced Colitis by Activating NLRP6 Signaling and

Regulating Th17/Treg Balance." *Phytomedicine* 107: 154452. https://doi.org/10.1016/j.phymed.2022.154452.

D'haens, G. R., and C. Jobin. 2019. "Fecal Microbial Transplantation for Diseases Beyond Recurrent *Clostridium difficile* Infection." *Gastroenterology* 157, no. 3: 624–636. https://doi.org/10.1053/j.gastro.2019.04.053.

Dubuquoy, L., E. A. Jansson, S. Deeb, et al. 2003. "Impaired Expression of Peroxisome Proliferator-Activated Receptor Gamma in Ulcerative Colitis." *Gastroenterology* 124, no. 5: 1265–1276. https://doi.org/10.1016/s0016-5085(03)00271-3.

Guo, C. S., S. J. Xie, Z. X. Chi, et al. 2016. "Bile Acids Control Inflammation and Metabolic Disorder Through Inhibition of NLRP3 Inflammasome." *Immunity* 45, no. 4: 802–816. https://doi.org/10.1016/j.immuni.2016.09.008.

He, Z., Y. Ma, S. Yang, et al. 2022. "Gut Microbiota-Derived Ursodeoxycholic Acid From Neonatal Dairy Calves Improves Intestinal Homeostasis and Colitis to Attenuate Extended-Spectrum β-Lactamase-Producing Enteroaggregative *Escherichia coli* Infection." *Microbiome* 10, no. 1: 79. https://doi.org/10.1186/s40168-022-01269-0.

Heiden, C. V. D., S. K. Wadman, P. K. D. Bree, and E. A. Wauters. 1972. "Increased Urinary Imidazolepropionic Acid, N-Acetylhistamine and Other Imidazole Compounds in Patients With Intestinal Disorders." *Clinica Chimica Acta* 39, no. 1: 201–214. https://doi.org/10.1016/0009-8981(72)90317-8.

Hu, J. Y., H. Huang, Y. Che, et al. 2021. "Qingchang Huashi Formula Attenuates DSS-Induced Colitis in Mice by Restoring Gut Microbiota-Metabolism Homeostasis and Goblet Cell Function." *Journal of Ethnopharmacology* 266: 113394. https://doi.org/10.1016/j.jep.2020.113394.

Hwang, Y. H., H. J. Yang, and J. Y. Ma. 2017. "Simultaneous Determination of Three Furanocoumarins by UPLC/MS/MS: Application to Pharmacokinetic Study of Angelica Dahurica Radix After Oral Administration to Normal and Experimental Colitis-Induced Rats." *Molecules* 22, no. 3: 416. https://doi.org/10.3390/molecules22030416.

Koh, A., A. Molinaro, M. Ståhlman, et al. 2018. "Microbially Produced Imidazole Propionate Impairs Insulin Signaling Through mTORC1." *Cell* 175, no. 4: 947–961.e17. https://doi.org/10.1016/j.cell.2018.09.055.

Li, D., Y. Feng, M. Tian, J. Ji, X. Hu, and F. Chen. 2021. "Gut Microbiota-Derived Inosine From Dietary Barley Leaf Supplementation Attenuates Colitis Through PPARγ Signaling Activation." *Microbiome* 9, no. 1: 83. https://doi.org/10.1186/s40168-021-01028-7.

Liang, Z., Z. Yin, X. Liu, et al. 2022. "A Glucomannogalactan From Pleurotus Geesteranus: Structural Characterization, Chain Conformation and Immunological Effect." *Carbohydrate Polymers* 287: 119346. https://doi.org/10.1016/j.carbpol.2022.119346.

Liu, M. J., G. H. Zhang, C. G. Zheng, et al. 2018. "Activating the Pregnane X Receptor by Imperatorin Attenuates Dextran Sulphate Sodium-Induced Colitis in Mice." *British Journal of Pharmacology* 175, no. 17: 3563–3580. https://doi.org/10.1111/bph.14424.

Lopes, S., G. Krausová, J. Carneiro, J. Gonçalves, R. Gonçalves, and A. De Oliveira. 2017. "A New Natural Source for Obtainment of Inulin and Fructo-Oligosaccharides From Industrial Waste of *Stevia rebaudiana* Bertoni." *Food Chemistry* 225: 154–161. https://doi.org/10.1016/j.foodchem.2016.12.100.

Magro, F., P. Gionchetti, R. Eliakim, et al. 2017. "Third European Evidence-Based Consensus on Diagnosis and Management of Ulcerative Colitis. Part 1: Definitions, Diagnosis, Extra-Intestinal Manifestations, Pregnancy, Cancer Surveillance, Surgery, and Ileo-Anal Pouch Disorders." *Journal of Crohn's & Colitis* 11, no. 6: 649–670.

Molinaro, A., P. B. Lassen, M. Henricsson, et al. 2020. "Imidazole Propionate Is Increased in Diabetes and Associated With Dietary Patterns and Altered Microbial Ecology." *Nature Communications* 11, no. 1: 5881. https://doi.org/10.1038/s41467-020-19589-w.

Ng, S. C., H. Y. Shi, N. Hamidi, et al. 2017. "Worldwide Incidence and Prevalence of Inflammatory Bowel Disease in the 21st Century: A Systematic Review of Population-Based Studies." *Lancet* 390, no. 10114: 2769–2778. https://doi.org/10.1016/S0140-6736(17)32448-0.

Qu, Y. F., X. Li, F. Xu, et al. 2021. "Kaempferol Alleviates Murine Experimental Colitis by Restoring Gut Microbiota and Inhibiting the LPS-TLR4-NF-κB Axis." *Frontiers in Immunology* 12: 679897. https://doi.org/10.3389/fimmu.2021.679897.

Rousseaux, C., B. Lefebvre, L. Dubuquoy, et al. 2005. "Intestinal Antiinflammatory Effect of 5-Aminosalicylic Acid Is Dependent on Peroxisome Proliferator–Activated Receptor-γ." *Journal of Experimental Medicine* 201, no. 8: 1205–1215. https://doi.org/10.1084/jem.20041948.

Shin, J. H., Y. K. Lee, W. J. Shon, et al. 2020. "Gut Microorganisms and Their Metabolites Modulate the Severity of Acute Colitis in a Tryptophan Metabolism-Dependent Manner." *European Journal of Nutrition* 59, no. 8: 3591–3601. https://doi.org/10.1007/s00394-020-02194-4.

Smolinska, S., M. Jutel, R. Crameri, and L. O'mahony. 2013. "Histamine and gut mucosal immune regulation." *Allergy* 69, no. 3: 273–281. https://doi.org/10.1111/all.12330.

Stephanie, A. C., L. Jee-Yon, M. V. Eric, et al. 2021. "5-Aminosalicylic Acid Ameliorates Colitis and Checks Dysbiotic *Escherichia coli* Expansion by Activating PPAR-γ Signaling in the Intestinal Epithelium." *MBio* 12, no. 1: e03227-20. https://doi.org/10.1128/mBio.03227-20.

Sun, M. M., W. Wu, Z. J. Liu, and Y. Z. Cong. 2016. "Microbiota Metabolite Short Chain Fatty Acids, GPCR, and Inflammatory Bowel Diseases." *Journal of Gastroenterology* 52, no. 1: 1–8. https://doi.org/10.1007/s00535-016-1242-9.

Teng, S. S., Y. F. Zhang, X. H. Jin, et al. 2023. "Structure and Hepatoprotective Activity of Usp10/NF-κB/Nrf2 Pathway-Related Morchella Esculenta Polysaccharide." *Carbohydrate Polymers* 303: 120453. https://doi.org/10.1016/j.carbpol.2022.120453.

Vieira-Silva, S., J. Sabino, M. Valles-Colomer, et al. 2019. "Quantitative Microbiome Profiling Disentangles Inflammation- and Bile Duct Obstruction-Associated Microbiota Alterations Across PSC/IBD Diagnoses." *Nature Microbiology* 4, no. 11: 1826–1831. https://doi.org/10.1038/s41564-019-0483-9.

Wang, B., J. Cao, B. Zhang, and H. Chen. 2019. "Structural Characterization, Physicochemical Properties and α-Glucosidase Inhibitory Activity of Polysaccharide From the Fruits of Wax Apple." *Carbohydrate Polymers* 211: 227–236. https://doi.org/10.1016/j.carbpol.2019.02.006.

Wang, J. M., P. L. Lian, Q. Yu, J. F. Wei, and W. Y. Kang. 2017. "Purification, Characterization and Procoagulant Activity of Polysaccharides From Angelica Dahurice Roots." *Chemistry Central Journal* 11: 17. https://doi.org/10.1186/s13065-017-0243-y.

Wang, J. Y., H. L. Wang, H. L. Zhang, Z. H. Liu, C. Y. Ma, and W. Y. Kang. 2019. "Immunomodulation of ADPs-1a and ADPs-3a on RAW264.7 Cells Through NF-κB/MAPK Signaling Pathway." *International Journal of Biological Macromolecules* 132: 1024–1030. https://doi.org/10.1016/j.ijbiomac.2019.04.031.

Wang, Y. J., Q. M. Li, X. Q. Zha, and J. P. Luo. 2022. "Intervention and Potential Mechanism of Non-starch Polysaccharides From Natural Resources on Ulcerative Colitis: A Review." *International Journal of Biological Macromolecules* 210: 545–564. https://doi.org/10.1016/j.ijbiomac.2022.04.208.

Wechsler, J. B., A. Szabo, C. L. Hsu, et al. 2018. "Histamine Drives Severity of Innate Inflammation via Histamine 4 Receptor in Murine Experimental Colitis." *Mucosal Immunology* 11, no. 3: 861–870. https://doi.org/10.1038/mi.2017.121.

Wu, Z. H., S. M. Huang, T. T. Li, et al. 2021. "Gut Microbiota From Green Tea Polyphenol-Dosed Mice Improves Intestinal Epithelial

Homeostasis and Ameliorates Experimental Colitis." *Microbiome* 9, no. 1: 184. https://doi.org/10.1186/s40168-021-01115-9.

Xu, S. F., Y. P. Ye, X. Y. Li, and F. Y. Chen. 2011. "Chemical Composition and Antioxidant Activities of Different Polysaccharides From the Roots of Angelica Dahurica." *Chemistry & Biodiversity* 8, no. 6: 1121–1131. https://doi.org/10.1002/cbdv.201000233.

Zhang, D., F. Ge, J. Ji, et al. 2023. "β-Sitosterol Alleviates Dextran Sulfate Sodium-Induced Experimental Colitis via Inhibition of NLRP3/Caspase-1/GSDMD-Mediated Pyroptosis." *Frontiers in Pharmacology* 14: 1218477. https://doi.org/10.3389/fphar.2023.1218477.

Zhu, M., R. Huang, P. Wen, et al. 2021. "Structural Characterization and Immunological Activity of Pectin Polysaccharide From Kiwano (*Cucumis metuliferus*) Peels." *Carbohydrate Polymers* 254: 117371. https://doi.org/10.1016/j.carbpol.2020.117371.

Supporting Information

Additional supporting information can be found online in the Supporting Information section.